Journal of Materials Science: Materials in Engineering

ORIGINAL PAPER Open Access

Optimization of silver nanoparticles synthesis using *Elaeis guineensis* Jacq. residue extract and their antibacterial activity against *Pseudomonas aeruginosa*

Jorge Benjamín Diaz-López[1], Diana De la Cruz-Gumeta[1], Gabriela Alvarado-Arguello[1], Oscar Rico-Domínguez[1], Evelyn Valdez-Rodríguez[1], Karina Hernández-Ovalle[2], María Celina Luján-Hidalgo[1], Rosa Isela Cruz-Rodríguez[1] and Rocío Meza-Gordillo[1*]

Abstract

This study explores the green synthesis of silver nanoparticles (Ag NPs) using oil palm (*Elaeis guineensis*) residue as a reducing agent. The synthesis was optimized by analyzing the effects of pH, silver nitrate ($AgNO_3$) concentration, and extract-to-$AgNO_3$ ratios using a Taguchi L9 design. The highest yield theorist (72%) was achieved under the conditions of pH 10, 100 mM $AgNO_3$ concentration, and a 2:3 extract-to-$AgNO_3$ ratio. The synthesized Ag-NPs were characterized through UV–Vis (400–450 nm), Fourier-transform infrared spectroscopy (FT-IR, 1370 cm^{-1}, attributed to the nitro group), dynamic light scattering (DLS, 10.07 nm average particle size with a hydrodynamic diameter (Dh) of 235.82 nm in a neutral pH), zeta potential (− 18.33 mV), scanning electron microscopy (SEM), and X-ray diffraction (XRD). Antimicrobial testing against *Pseudomonas aeruginosa* revealed antibacterial activity, making these nanoparticles a promising alternative to traditional antibiotics.

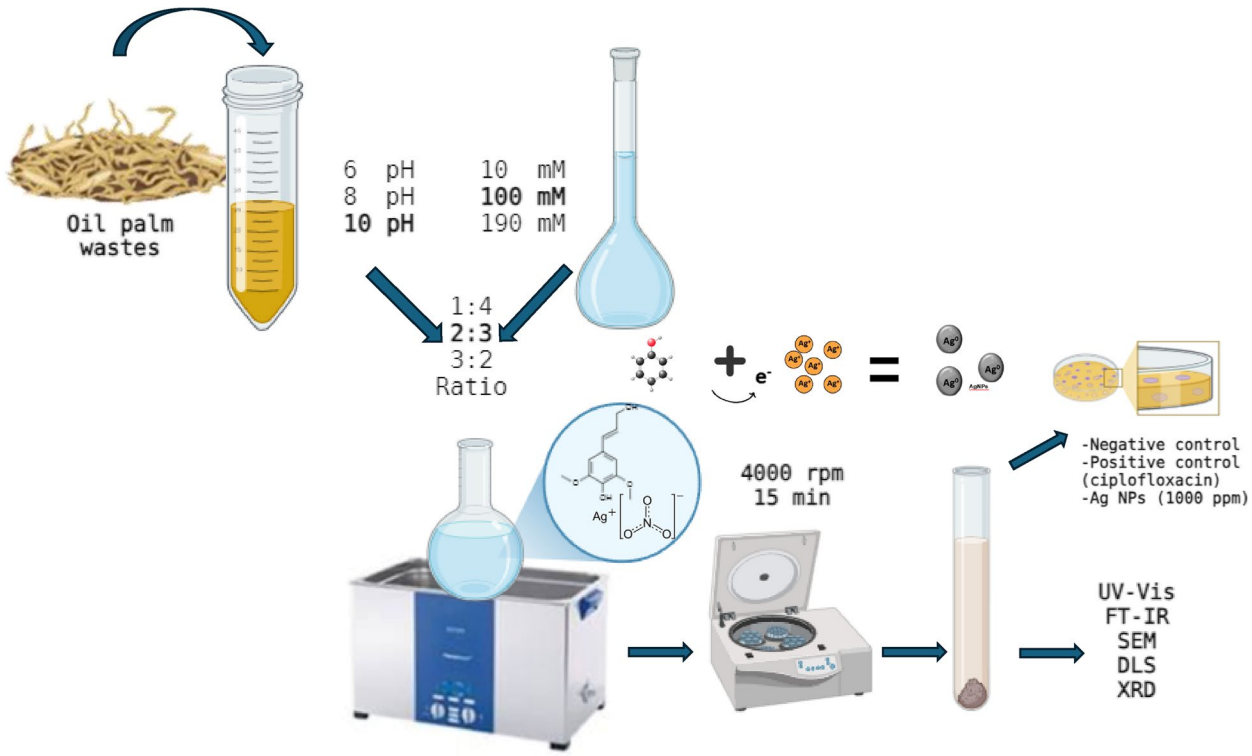
Keywords Residual biomass, Oil palm, Palm husks

*Correspondence:
Rocío Meza-Gordillo
rocio.mg@tuxtla.tecnm.mx
Full list of author information is available at the end of the article

Springer Open

© The Author(s) 2025. **Open Access** This article is licensed under a Creative Commons Attribution 4.0 International License, which permits use, sharing, adaptation, distribution and reproduction in any medium or format, as long as you give appropriate credit to the original author(s) and the source, provide a link to the Creative Commons licence, and indicate if changes were made. The images or other third party material in this article are included in the article's Creative Commons licence, unless indicated otherwise in a credit line to the material. If material is not included in the article's Creative Commons licence and your intended use is not permitted by statutory regulation or exceeds the permitted use, you will need to obtain permission directly from the copyright holder. To view a copy of this licence, visit http://creativecommons.org/licenses/by/4.0/.

Graphical Abstract



Introduction

The oil palm industry generates a substantial volume of by-products year-round, particularly during palm oil production, leading to a considerable accumulation of organic residues such as husks, fibers, and shells (Ong et al. 2021). These residues pose environmental challenges and contribute to high operational costs for the oil processing sector. Issues such as rapid decomposition, limited disposal sites, and high transportation expenses further complicate effective waste management (Nabila et al. 2023). Consequently, the need to valorize and reutilize oil palm by-products presents a promising pathway toward sustainability in the palm oil industry (Anyaoha et al. 2018).

Among these by-products, oil palm husks constitute a significant portion of the waste, with annual production volumes reaching millions of tons (Kahar et al. 2022). Beyond their sheer abundance, these husks are of considerable biotechnological interest due to their rich content of bioactive compounds, such as polyphenols, which have demonstrated potential for diverse applications (Huan et al. 2022; Nuchdang et al. 2022). Advances in nanotechnology have increasingly highlighted the cost-effective and non-toxic advantages of using plant-based reducing agents for the green synthesis of silver nanoparticles (AgNPs) (Dzul-Erosa et al. 2018).

Elaeis guineensis Jacq., commonly known as the oil palm, has been utilized in the synthesis of various nanoparticles, including gold nanoparticles (AuNPs, ZnNps, TiO_2NPs) (Ahmad et al. 2017; Saputra et al. 2024; Putri et al. 2024), due to its rich phytochemical content. In this context, oil palm husks offer a sustainable and cost-effective alternative for AgNP production, leveraging their natural phenolic content to facilitate nanoparticle formation while simultaneously addressing the environmental burden of agricultural waste (Princy et al. 2023). Silver has been used as a microbial inhibitor (Mazariegos et al. 2019), and it is now possible to modify this metal to a nanometric size, resulting in silver nanoparticles (Ag NPs) (Thakur et al. 2024). Silver nanoparticles have garnered significant attention due to their potent antimicrobial properties, which are particularly valuable in combating multidrug-resistant pathogens.

The antimicrobial activity of AgNPs is attributed to several mechanisms that disrupt microbial cells and inhibit their growth as adhesion and disruption of cell

membranes, intracellular penetration and damage, generation of reactive oxygen species, and modulation of signal transduction pathways (Dakal et al. 2016). Due to their wide range of applications, Ag NPs are used in drug development, biological systems, and as antiviral, anticancer, antibacterial agents, as well as catalysts and in optoelectronics (Shantkriti et al. 2023; Aravind et al. 2021). There are various methods for the green synthesis of Ag NPs; however, it has been shown that the reaction yield can vary depending on the reaction conditions employed (Nangare and Patil 2020).

A substantial amount of research has been dedicated to the green or plant-mediated synthesis of silver nanoparticles. The physicochemical characteristics of silver nanoparticles are crucial in determining their antibacterial and cytotoxic effects (Bamal et al. 2021). pH concentration of plant metabolites as reducing agents, temperature, and silver ion concentration have been evaluated as conditions to synthesize AgNPs (Habeeb et al. 2022; Ahmed and Mustafa 2020).

The integration of green synthesis methods and the detailed characterization of nanoparticles can lead to significant advancements in controlling resistant bacterial infections caused by *Pseudomonas aeruginosa* that is a significant opportunistic pathogen known for causing severe infections, particularly in immunocompromised individuals and patients with cystic fibrosis. Its ability to develop resistance to multiple antibiotics poses a major challenge in clinical settings and contribute to the sustainable development of nanomaterial technologies (Jiménez et al. 2023; Villani et al. 2024). In the present work, the optimization of the synthesis of Ag NPs using extracts from *Elaeis guineensis* Jacq. residues and it is antimicrobial acitivity against *Pseudomonas aeruginosa* were proved.

Materials and methods

Elaeis guineensis Jacq. extract conditions

The oil palm (*Elaeis guineensis* Jacq.) husk wastes were provided by Propalma, a company located in Acapetahua, Chiapas, Mexico. The residues were dried at 60 ± 2 °C, ground, and sieved (n°35; < 0.5 mm). For the extraction of oil palm husk extract, a 1:5 ratio (residue-distilled water) was used. Sonication was carried out in a simple frequence ultrasonic bath TEBU-3L (Felisa, Mexico) with 40 kHz ultrasound frequency, 120 W of ultrasound power, and 100 W of heating power, for 1 h at 50 °C (Ofori-Boateng and Lee 2013), followed by filtration and centrifugation at 4000 rpm for 15 min. Subsequently, the pH was adjusted to pH 7 with a 10 mM NaOH solution. The procedure was performed in the absence of light.

Experimental design for the synthesis of Ag NPs

The effect of $AgNO_3$ concentration (10, 100, and 190 mM); pH (6, 8, and 10); and extract-$AgNO_3$ ratio (1:5, 2:5, and 3:5) on the synthesis yield of Ag NPs was evaluated using a Taguchi L9 orthogonal design. The Taguchi L9 experimental design is a robust optimization method that allows for the systematic evaluation of the effects of multiple factors on a process while minimizing the number of experimental trials. In this study, a Taguchi L9 orthogonal array is employed to assess the influence of three factors: $AgNO_3$ concentration, pH, and extract-$AgNO_3$ ratio, each with three levels. The L9 design consists of 9 experimental trials, as it is based on an orthogonal array that allows the efficient investigation of these factors and their interactions. Three levels are selected for $AgNO_3$ concentration (10 mM, 100 mM, and 190 mM). This factor evaluate the effect of varying the concentration of $AgNO_3$ on the desired outcome. The pH of the solution is crucial for understanding how pH affects the synthesis or behavior of the reaction in the presence of the extract and $AgNO_3$. Extract-$AgNO_3$ ratio evaluate how the proportion of extract relative to $AgNO_3$ influences the process. The Taguchi L9 design involves 9 experimental combinations, each corresponding to one of the following sets of factor levels (Table 1).

This design enables the study of individual and interactive effects of these factors while maintaining a minimal number of experimental trials. By using this approach, it is possible to identify the optimal conditions for the desired outcome with greater efficiency and less resource usage.

The response variable was the theoretical yield. The results were statistically analyzed using a completely randomized one-way analysis of variance (ANOVA) with a significance level of $p < 0.05$ based on a polynomial equation. A Tukey test was used for mean comparisons with

Table 1 Nine trials based on the different levels of $AgNO_3$ concentration, pH and extract $AgNO_3$ ratio

Trial	$AgNO_3$ conc. (mM)	pH	Extract-$AgNO_3$ ratio
1	10	6	1:5
2	10	8	2:5
3	10	10	3:5
4	100	6	2:5
5	100	8	3:5
6	100	10	1:5
7	190	6	3:5
8	190	8	1:5
9	190	10	2:5

95% confidence, using Minitab 17 software. The general synthesis was as follows: 30 mL of the corresponding concentration solution of $AgNO_3$ was added to an Erlenmeyer flask immersed in a sonicator at 60 °C, followed by the dropwise addition of 20 mL of *Elaeis guineensis* Jacq. extract. The solution was then stirred at 50 °C on a hot plate for 1 h, with samples taken every 15 min, diluted with distilled water in a 1:4 ratio to measure their absorbance in a UV–Vis spectrophotometer.

Characterization of Ag NPs

The characterization of the Ag NPs was performed using UV–Vis spectroscopy SP500-UV (Cole Parmer, Vernon Hills, USA), with a Xenon lamp, single beam type, 2 nm bandwith, minimum wavelength (nm) 198, maximum wavelength (nm) at 800, and wavelength accuracy ± 2 nm. The Fourier-transform infrared spectroscopy (FT-IR) were recorded using a Nicolet™ IR spectrophotometer (Thermo Scientific, MA, USA). The spectra were obtained in the range of 650–4000 cm^{-1} with a resolution of 4 cm^{-1} [50]. The samples were placed directly into the FTIR. Dynamic light scattering (DLS) and zeta potential analysis were done in a Horiba Scientific DLS SZ-100, particle size: 0.3 nm–8 µm, diode laser 532 nm, zeta potential range − 200 mV a + 200 mV; the surface morphology scanning electron microscopy (SEM) was characterized using an acceleration voltage of 15 to 20 kV (Zeiss Gemini Auriga, Oberkochen, Germany) at 25 kV, the samples were introduced into the analyzer, and electron micrographs were captured for each sample at various magnifications. The X-ray diffraction patterns were obtained using a powder diffractometer (Rigaku, Ultima IV, Tokyo, Japan) with Cu-Kα radiation as the source, operated at 44 kV and 300 mA. Scattered radiation was detected in the range of $2\theta = 10–40°$ at a scanning speed of 2°/min and antibacterial activity assay as described below.

Antibacterial activity assay

Pseudomonas aeruginosa (ATCC 27853), used for the antibacterial activity assay, was maintained in tryptic soy agar (TSA) (MCD LAB, Mexico City, Mexico), incubated at 37 °C, and cryopreserved in glycerol-tryptic soy broth. Once reactivated in TSA at 37 °C, 3.8 g of Mueller–Hinton agar were dissolved in 100 mL of distilled water with constant stirring until a yellow crystalline solution was obtained. The mixture was then poured into Petri dishes, which were sealed and allowed to stand for 24 h. For the inoculation of *Pseudomonas aeruginosa*, a sterile inoculating loop was used to collect a bacterial sample from culture medium. The loop was carefully streaked onto the surface of the solidified Mueller–Hinton agar to distribute the bacteria. The inoculated plates were then incubated at 37 °C for 48 h (Festus and Emmanuella 2020). Ag NPs were applied to the center of the plates at a concentration of 1000 ppm. A positive control (ciprofloxacin at 5000 ppm) and a negative control (water) were also included. The inhibition of AgNPs was measured as the presence or absence of *Pseudomonas aeruginosa* growth.

This manuscript was for grammar and spelling using ChatGPT (Open AI, USA). The LLM was used solely for language refinment, and no changes were made to the scientific content or the interpretation of the results.

Results and discussion

Ag NPs synthesis optimization

After performing the statistical analysis ($p \leq 0.05$) of the results, the optimal treatment is presented with a pH of 10, and $AgNO_3$ concentration of 100 mM, with no significant statistical effect compared to 190 mM, and a 2:3 extract-$AgNO_3$ ratio, yielding 72% and an R^2 of 82% (Fig. 1). Siddiqui et al. (2018) states that the synthesis of silver nanoparticles initially begins when $AgNO_3$ dissociates into Ag^+ ions. These silver cations disperse in the aqueous solution, and the hydroxyl groups of phenolic compounds act as a capping agent, covering the surface of the silver nanoparticles. In this way, the colloidal stabilization of silver occurs, possibly due to Van der Waals forces between the negatively charged oxygen (δ^-) and the positively charged groups surrounding the surface of the Ag NPs (Huan et al. 2022). The formation of Ag NPs can be observed through the color change of the synthesis (yellow, orange, and brown) when the extract comes into contact with $AgNO_3$, with the intensity of the color change increasing over the synthesis time. This color change occurs due to the excitation vibrations of the surface plasmon on the metal nanoparticles (Kiba et al. 2021). The significant effects observed at pH 10 and high $AgNO_3$ concentrations during nanoparticle synthesis can be attributed to the altered chemical environment that influences silver ion reduction, nucleation, and particle growth. At pH 10, the increased availability of hydroxide ions (OH^-) facilitates the formation of silver hydroxide (AgOH), which may act as a precursor for nanoparticle formation (Hasan et al. 2024). Additionally, alkaline conditions enhance the reduction kinetics of Ag^+ to Ag^0, leading to efficient nucleation. The high $AgNO_3$ concentration provides a greater supply of silver ions, increasing nucleation sites but potentially affecting size distribution due to rapid growth (Gangwar et al. 2021). Furthermore, electrostatic stabilization at high pH prevents excessive aggregation, contributing to the formation of well dispersed nanoparticles (Ji et al. 2021). This synthesis was carried out using the precursor solution of $AgNO_3$ and the *Elaeis guineensis* Jacq. extract adjusted to the established pH, acting as a reducing agent through the –OH groups

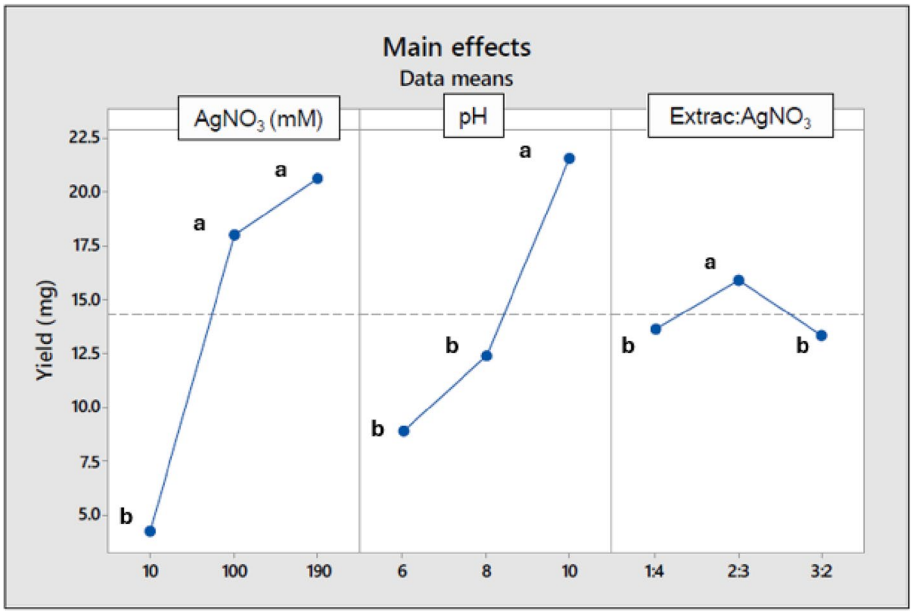


Fig. 1 Overview of the effects of key experimental factors on the synthesis, morphology and yield of silver nanoparticles (AgNPs)

of phytoconstituents (such as flavonoids or other polyphenols, some of which include gallic acid, flavon-3-ol, flavon-4-ol, and flavon-3,4-diol), these compounds act as electron donors, facilitating the reduction of metal ions (e.g., Ag^{+} or Au^{3+}) into their zero-valent metallic form (Ag^{0} or Au^{0}), (Shantkriti et al. 2023; Siddiqui et al. 2018; Alharbi et al. 2022; Chugh et al. 2021; Habeeb et al. 2022).

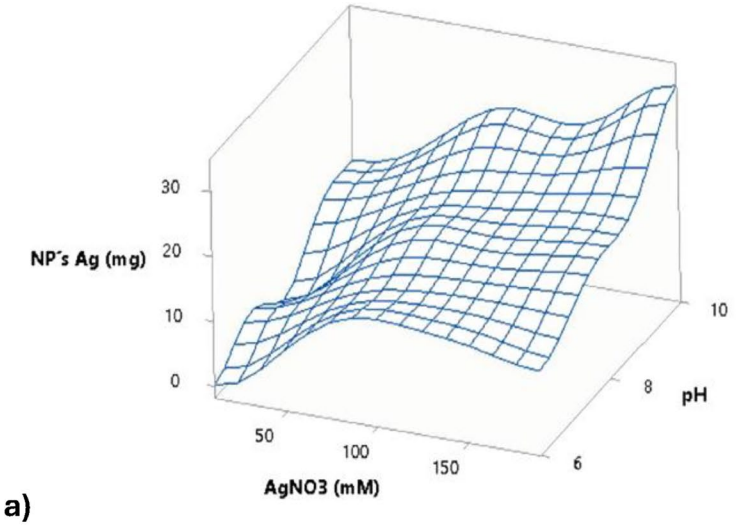
According to the statistical analysis, the linear regression equation was obtained (Eq. 1); this was done in order to predict the Ag NPs yield values based on pH, $AgNO_3$ concentration, and the extract-to-$AgNO_3$ ratio.

$$\text{Ag NPs (mg)} = -19.91 + 3.172\ \text{pH} + 0.0906\ \text{AgNO}_3\ \text{(mM)} - 0.12\ \text{Extract} : \text{AgNO}_3 \quad (1)$$

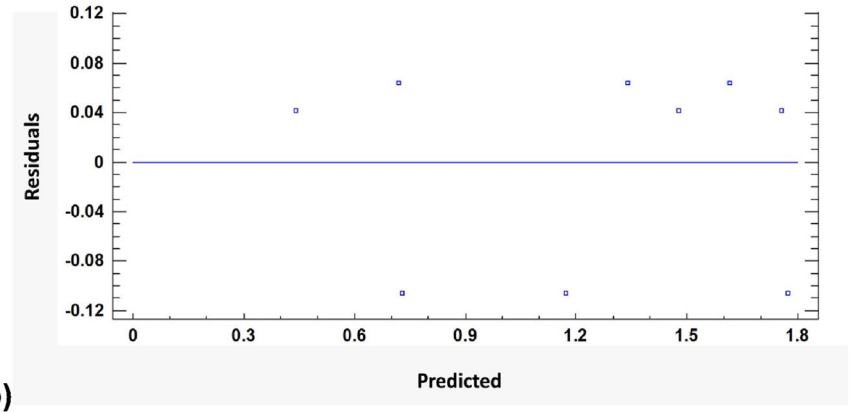
which is essential for nanoparticle nucleation. Once nanoparticles are formed, these biomolecules prevent excessive growth and aggregation by providing electrostatic and steric stabilization, the presence of multiple hydroxyl and carboxyl groups in gallic acid enhances hydrophilicity, which improves nanoparticle dispersion in aqueous media.

Flavonoids interact with the metal nanoparticle surface through π-electron interactions and hydrogen bonding, modulating their final shape and size. The number and position of hydroxyl groups in flavonoids can affect nanoparticle size distribution, leading to uniform or polydisperse particles depending on reaction conditions, acting as capping agents influence the morphology of nanoparticles by controlling their growth and preventing excessive coalescence. With the assistance of the bioactive compounds present in the synthesis, this leads to the coprecipitation of the Ag NPs. This formation results in nucleation, meaning an aggregation of the nanoparticles with the bioactive compounds present in the *Elaeis guineensis* Jacq. extract

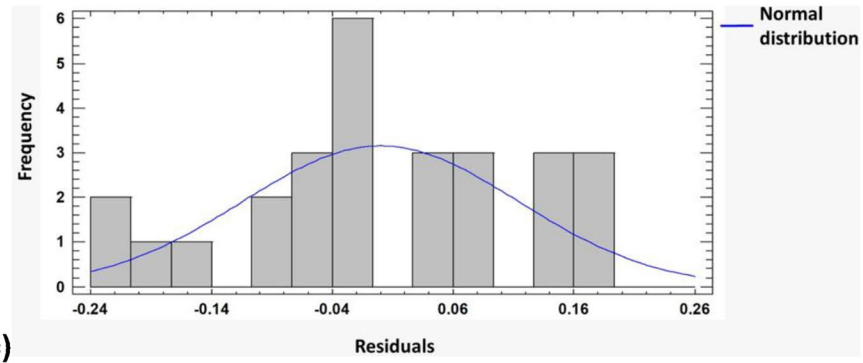
As shown in Fig. 2a, the surface plot illustrates the effect of pH in relation to $AgNO_3$ concentration. A higher pH and $AgNO_3$ concentrations of 100 and 190 mM have significant statistical effect ($p \leq 0.05$) for higher Ag NPs yield. The model was based on 49 observations (based on the degrees of freedom in the ANOVA: $16+32+1$). The residual plot (2b) shows that the residuals range between -0.12 and 0.12, with most values close to zero, indicating that the model predicts well. There is no evident pattern of increasing or decreasing spread, which suggests that the variances are constant. The distribution appears symmetric, supporting normality and suggesting that the model assumptions are met. The non-normality of the residuals (2c) ($p = 0.037 < 0.05$) indicates that one of the key assumptions of linear regression is not fully met. The data simply do not meet the assumption of normality of the residuals. This is common and does not automatically invalidate the analysis. An attempt was made to correct the non-normality ($p = 0.037$) using a transformation such as Box-Cox, resulting in a p-value of 0.087.



a)



b)



c)

Fig. 2 Influence of pH and the extract-to-$AgNO_3$ ratio on the yield of silver nanoparticles (AgNPs), highlighting how variations in these parameters affect nanoparticle formation efficiency and overall synthesis outcome. **a** Three-dimensional surface response plot for the synthesis of Ag NPs as a function of $AgNO_3$ concentration and pH. The panel shows the combined influence of both variables on the number of nanoparticles obtained. **b** Residuals versus predicted values plot for the regression model applied to the synthesis of Ag NPs. The random distribution of residuals around zero indicates that the model fits the experimental data well, with no evident systematic patterns. **c** Histogram of residuals overlaid with the normal distribution curve. The closeness of the histogram shape to the normal curve suggests that the model residuals are approximately normally distributed, which supports one of the fundamental assumptions of regression analysis

pH effect on the synthesis of Ag NPs

The pH has statistically significant effect ($p \leq 0.05$) on the yield and production of Ag NPs. It was observed that an alkaline pH (pH 10) is optimal for the synthesis conditions. The synthesis of AgNPs is highly pH-dependent. Studies have shown that a pH of around 8 to 10 is often optimal for producing smaller and more uniform nanoparticles. According to Quintero-Quiroz et al. (2019), a pH of 8 resulted in a high yield of AgNPs with a diameter less than 10.30 nm. Nelagadarnahalli et al. (2023) reported optimal synthesis at pH 10, resulting in bimodal size distribution with diameters of 7.3 nm and 14.3 nm. Similarly, pH levels of 8 and 9 were found to be effective for producing nanoparticles with sizes between 25 and 30 nm. Various methods presented in the literature indicate that the morphology and size of Ag NPs depend on the pH of the reducing agent (Lima et al. 2022; Smirnov et al. 2023). These characteristics are directly affected by the adjusted pH, which is evident when observing the color changes, ranging from colorless to brown. According to Chugh et al. (2021), this is due to the concentration of electric charges from the reducing agents present in the plant extract, which are strongly altered under different pH conditions, affecting their ability to bind and reduce metal ions. In the evaluation of different pH levels in the synthesis of Ag NPs, Gontijo et al. (2020) highlighted the dependence of Ag NPs on pH. Additionally, through this variation, it was possible to observe greater aggregation within the pH range of 3 to 7. At pH levels below 3 and above 7, less aggregation was observed. Based on this study, it was confirmed that the stability of Ag NPs is highly influenced by pH. A potential influence was also determined between the synthesis of Ag NPs at alkaline pH and their microbial inhibition potential (Gontijo et al. 2020).

$AgNO_3$ concentration effect on the synthesis of Ag NPs

The concentration of the precursor salt ($AgNO_3$), according to the statistical analysis, has significant statistical effect ($p \leq 0.05$). The highest yield of the synthesized nanoparticles was obtained using concentrations of 100 mM and 190 mM, with no significant statistical difference between them. According to Chugh et al. (2021), this concentration directly influences the yield of the synthesized nanoparticles, meaning that the higher the concentration, the greater the yield, due to the presence of silver cations in the reaction. Rahman et al. (2019), in their evaluation of two concentrations, one low and one high, note that a high concentration of $AgNO_3$ could promote the synthesis of Ag NPs with smaller sizes and higher yields, in contrast to using lower concentrations. This is due to the reactions between the reducing compounds of the extract, which come into contact with a higher number of silver cations. Therefore, it is of interest to understand the relationship between the extract and silver ion concentration. Lower concentrations have been associated with optimal nanoparticle synthesis. For example, a concentration of 1 mM $AgNO_3$ at pH 8 yielded nanoparticles with significant biological activity (Nelagadarnahalli et al. 2023). Another study found that a concentration of 0.8 mM $AgNO_3$ at pH 5 produced quasi-spherical nanoparticles with a mean diameter of 16.63 nm (Rose et al. 2023).

Extract: $AgNO_3$ ratio effect on the synthesis of Ag NPs

The effect of the extract: $AgNO_3$ ratio is undoubtedly evident, according to the relationship between reactant and the generated product (Ag NPs). There must be an equilibrium in the ratio, depending on the content of compounds in the extract

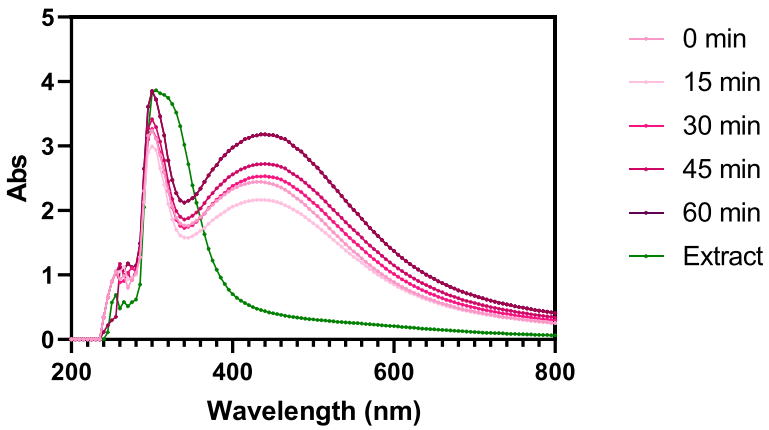


Fig. 3 UV–Vis spectra of *Elaeis guineensis* extract monitored during the synthesis of silver nanoparticles (AgNPs), illustrating the progression of nanoparticle formation through characteristic surface plasmon resonance peaks over time

that will react with the silver cations in the $AgNO_3$ solution.

Characterization of Ag NPs

UV–Vis spectroscopy

The absorbance spectra can confirm the formation of silver nanoparticles synthesized in a solution. The estimated synthesis time was 1 h, as recorded in UV–VIS spectra (Fig. 3). It can be observed that, starting from the absorbance of the *Elaeis guineensis* Jacq. residue extract, which represents the transition from n to π* corresponding to the C-O bonds present in the phenolic compounds of the extract, when the extract comes into contact with $AgNO_3$, there is a change in the conformation of the chemical structure, thereby producing a new absorbance spectrum that leads to the formation of Ag NPs at a wavelength of 400–450 nm (Alharbi et al. 2022; Habeeb et al. 2022; Dhasarathan et al. 2018). Alharbi et al. (2022) describe a possible relationship between absorbance, wavelength, and the size of Ag NPs, due to the resonance of the silver plasmons. Lower wavelength values (400 nm or less) are associated with smaller average particle sizes, while higher wavelengths (450 nm or more) correspond to a higher concentration of Ag NPs, which is evident in a higher absorbance.

FT-IR (Fourier-transform infrared spectroscopy)

In Fig. 4, the first FT-IR spectrum shows the functional groups belonging to the *Elaeis guineensis* Jacq. residue extract; the characteristic band at 3300 cm^{-1} corresponds to the –OH group of the phytochemical compounds present in the extract, as well as the 1600 cm^{-1} band representing carbon double bonds. The second spectrum shows a signal at 1370 cm^{-1}, attributed to the nitro group of $AgNO_3$. The third spectrum, corresponding to the Ag NPs after synthesis and coprecipitation, shows a decrease in the 1370 cm^{-1} band from $AgNO_3$ and the –OH group, along with bands at 2925–2850 cm^{-1}, attributed to the stretching vibrations of aliphatic C–H bonds, specifically the asymmetric and symmetric stretching of $–CH_2$ and $–CH_3$ groups. Palm oil residues are rich in various organic compounds, including fatty acids, triglycerides, and other lipid-derived molecules. During the synthesis process, these biomolecules not only act as reducing agents for Ag^+ ions but also serve as capping agents that stabilize the surface of the nanoparticles. Therefore, the bands at 2925 and 2850 cm^{-1} provide strong evidence for the presence of long-chain hydrocarbon groups associated with these natural capping agents on the nanoparticle surface. The band at 1700 cm^{-1} corresponds to the carboxyl functional group. Their presence supports the successful bio-reduction and stabilization of AgNPs by the organic constituents in the palm oil residue extract.

DLS (Dynamic light scattering)

The average size of the Ag NPs was measured using dynamic light scattering (DLS) and was found to be 10.07 nm with a hydrodynamic diameter (Dh) of 235.82 nm and a polidispersity index (PDI) of 0.412 in a neutral pH, corresponding to the interaction/aggregation

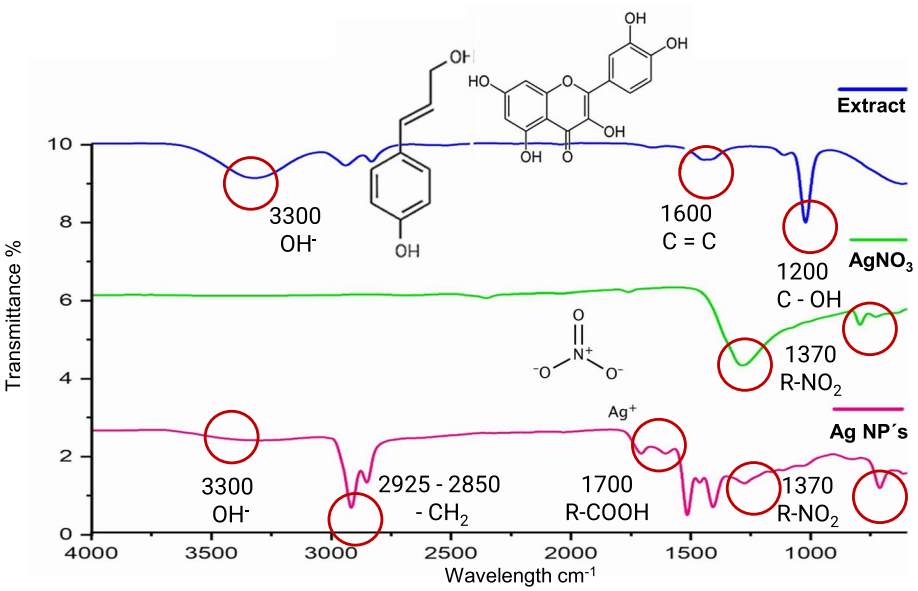


Fig. 4 FT-IR spectra of *Elaeis guineensis* residue extract, silver nitrate ($AgNO_3$), and synthesized silver nanoparticles (AgNPs), highlighting the functional groups involved in the reduction and stabilization of AgNPs

process of the Ag NPs due to the charge behavior of the surface plasmons (Villani et al. 2024), indicating a broad size distribution consistent with the presence of aggregates. This addition strengthens the explanation regarding particle aggregation and provides a more complete characterization of the system.

It is important to note that NPs tend to approach their isoelectric point in acidic solutions. This means that the surface charge is negative because, in an acidic solution, they are close to their isoelectric point and tend to behave as positive, due to the proton donation from the solution to the nanoparticles. In alkaline solutions, they tend to have a greater negative charge, making the nanoparticle charge negative, due to proton donation now from the bioactive compounds present on the nanoparticles. This analysis is of interest since the nanoparticle behavior will influence their potential applications.

The Dh will be influenced by the pH of the solution in which the nanoparticles are suspended. The other synthesis conditions like acidic pH, nanoparticles tend to aggregate more due to reduced electrostatic repulsion, leading to larger particle sizes and leading to a higher Dh and lower dispersion. This is because the surface charge of nanoparticles is often neutralized at lower pH, promoting aggregation. Conversely, the increased pH results in a higher surface charge, which enhances electrostatic repulsion between particles, thus reducing aggregation and leading to a smaller Dh in alkaline pH, there will be greater dispersion, resulting in a lower Dh (Fernando and Zhou 2019; Xiong et al. 2021; Gontijo et al. 2020; Horiba Scientific 2022).

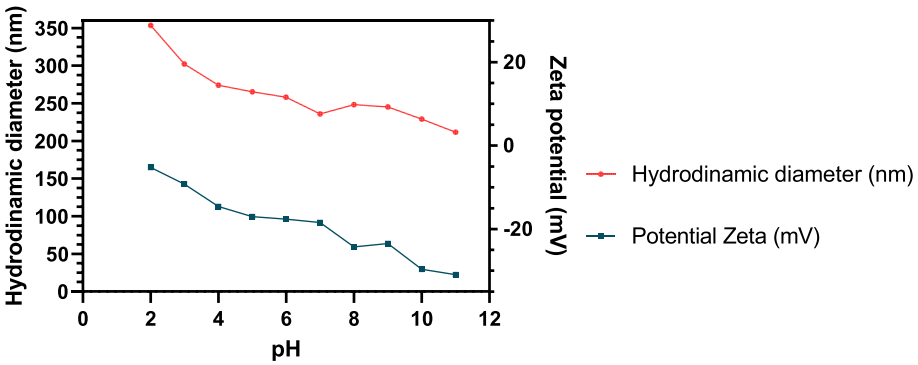


Fig. 5 Effect of pH on the hydrodynamic diameter (Dh) and zeta potential of silver nanoparticles (AgNPs) synthesized using *Elaeis guineensis*, demonstrating how pH influences particle size distribution and surface charge stability

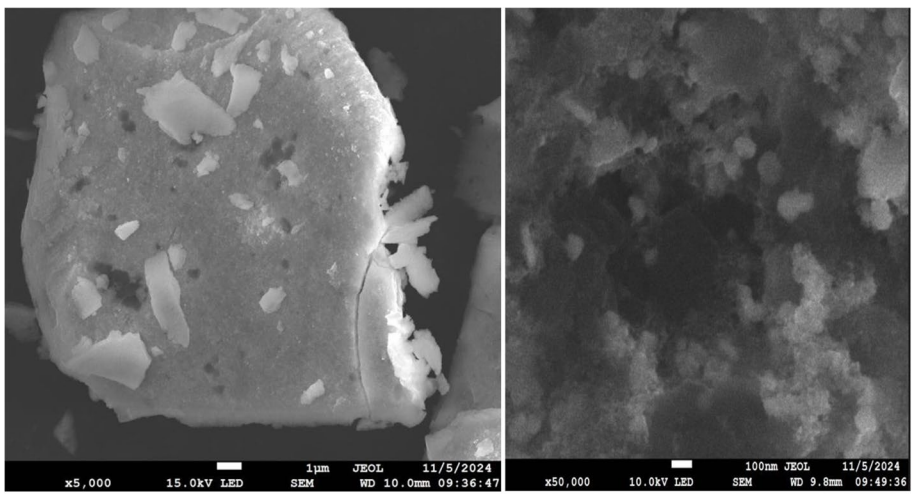


Fig. 6 Scanning electron microscopy (SEM) image of silver nanoparticles (AgNPs) synthesized using palm oil residues, captured at 5000× magnification, revealing the surface morphology. Scanning electron microscopy (SEM) image of silver nanoparticles (AgNPs) synthesized using palm oil residues, captured at **a**) 5000x magnification, and at **b**) 50,000x magnification, revealing the surface morphology

Zeta potential

The obtained zeta potential value was − 18.33 mV (Fig. 5), which is related to the Dh (Gasztych et al. 2024), as when zeta potential is less than ± 30 mV indicates a lower electrostatic repulsion between particles, which promotes aggregation and reduces stability in terms of size and charge (Ronávári et al. 2021; Meher et al. 2024). Aggregation, and consequently the sedimentation of particles, occurs when the particles have a charge of zero in relation to the suspension medium (Sharma et al. 2023; Luxbacher 2014). Therefore, at acidic pH, a lower zeta potential value will result in less dispersion and greater aggregation, while at alkaline pH, a higher zeta potential will have an effect on the polydispersity index of the Ag NPs, leading to greater dispersion and less aggregation (Dh) (Gontijo et al. 2020).

Scanning electron microscopy (SEM) and X-ray diffraction (XRD)

SEM images of the Ag NPs prepared in this study are shown in Fig. 6. The morphology of the Ag NPs is visualized with sizes that agree with the DLS analysis, as well as a irregular shape. We can observe the agglomeration of the nanoparticles (Fig. 6A), as well as the different approximate sizes of the Ag NPs (Fig. 6B). The presence of Ag NPs is evident due to their conductivity that will translate into the sharpness of the image, quite the opposite with organic compounds that are not coated with gold, their presence will be evidenced indirectly in the areas with greater brightness (Shantkriti et al. 2023; Alharbi et al. 2022; Chugh et al. 2021). The XRD patterns exhibit pronounced peaks (Fig. 7) corresponding to the crystallographic planes of the Ag NP surfaces. The results indicate a crystalline structure of the Ag NPs, with peaks that closely match those of pure silver (ICSD 01–071–6549). According to Dzido et al. (2015), these correspond to the (111), (200), (220), (311), and (222) planes of face-centered cubic (FCC) silver crystals (Alharbi et al., 2022; Dzido et al., 2015).

Likewise, we can observe in the work of Ödemiş et al. (2022) the presence of Ag NPs is determined by X-ray diffraction with the same crystallographic chart and sizes corresponding to those observed in this study in DLS (Ödemiş et al. 2022) are obtained; in that work, the presence of silver bound with another molecule with peaks of lower intensity is observed, which coincide with ours indicated in blue, which express a product formed by the reaction of $AgNO_3$ and the bioactive compounds of the extract; in this study, it was determined as polyvinyl alcohol (PVA) bound to Ag NPs according to crystallographic chart 00–058–1068; however, it is necessary to do a more detailed study of the presence of this in the synthesis of

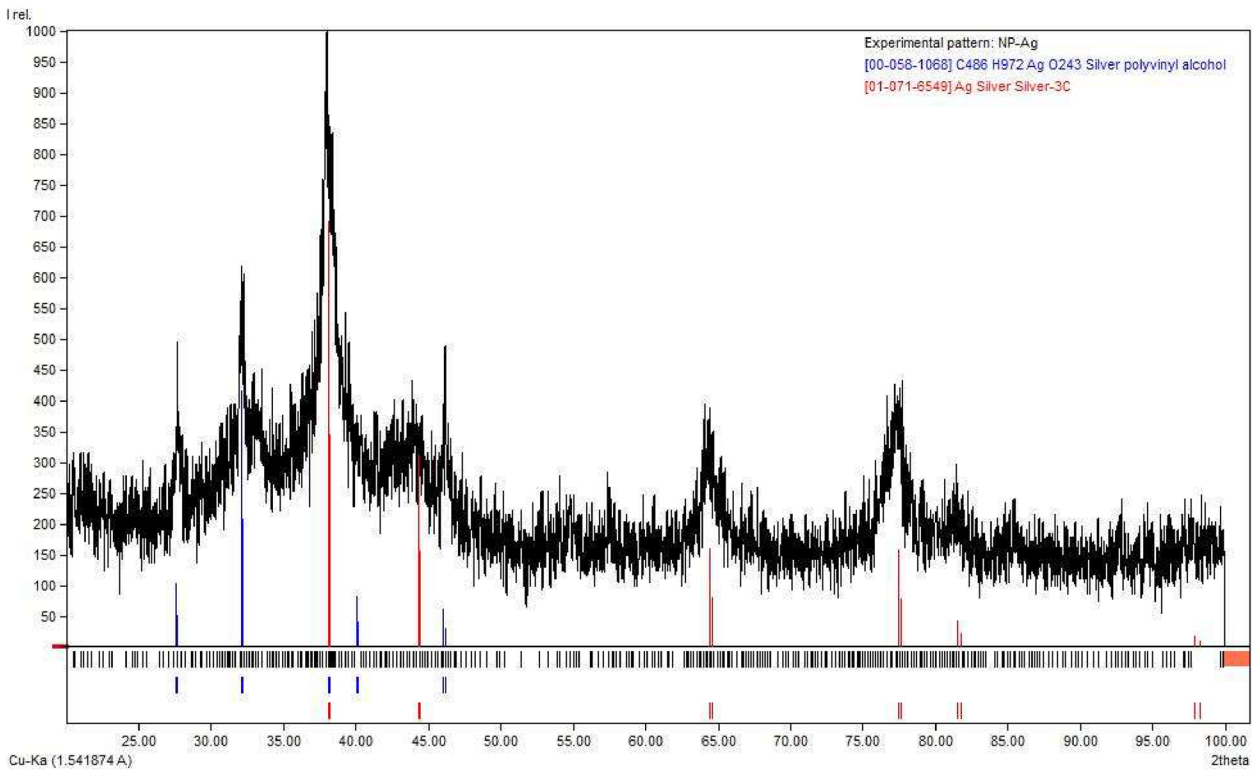
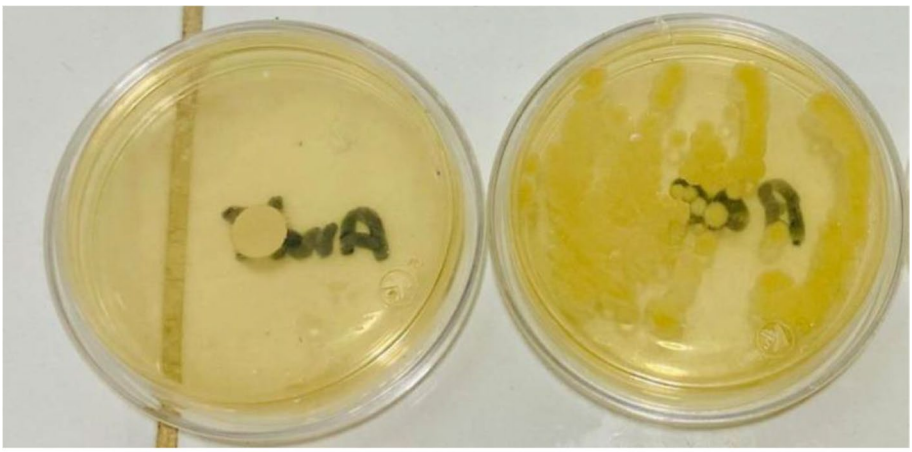


Fig. 7 X-ray diffraction (XRD) patterns of silver nanoparticles (AgNPs), illustrating their crystalline structure and phase composition



A B

Fig. 8 Antimicrobial activity assays of silver nanoparticles against *P. aeruginosa*, demonstrating their inhibitory effects on bacterial growth. Antimicrobial activity assays of silver nanoparticles against P. aeruginosa, **a**) 1000 ppm AgNP's, **b**) negative control (distilled water), demonstrating their inhibitory effects on bacterial growth.

Ag NPs (Ödemiş et al. 2022). The interactions between AgNPs and PVA significantly influence the stability, optical, antibacterial, antioxidant, mechanical, and biocompatibility properties of the resulting nanocomposites. These interactions are primarily driven by the stabilizing role of PVA, which binds to AgNPs through its hydroxyl groups, enhancing the overall performance (Velgosova et al. 2023). The average crystallite size from the XRD data using the Scherrer formula was 16.29 nm.

Activity assays against *P. aeruginosa*

The results in the three treatments: (Fig. 8) negative control (distilled water, B) and 1000 ppm of Ag NPs (A), it was observed that the treatment with 1000 ppm inhibited at 100% the growth of *Pseudomonas aeruginosa*, compared to the negative control. Although the plant itself has an antibacterial effect, it is promising for the green synthesis with Ag in nanometric sizes since this could increase its antibacterial potential, due to its biocompatibility by remaining bound to bioactive compounds belonging to the plant extract. The antibacterial properties of $AgNO_3$ have been well-documented (Klasen 2000). Therefore, its use as a precursor salt in the synthesis of AgNPs presents a promising alternative. The results suggest that this approach could be extended beyond *Pseudomonas aeruginosa* to include Gram-positive bacteria and even yeasts, broadening the scope of antimicrobial studies (Chouhan and Guleria 2020; Wang et al. 2022). These can be attributed to what was reported by Habeeb et al. (2022) that the antibacterial activity of nanoparticles will depend on their stability, size, and shape; this is because silver nanoparticles, which are smaller, have more binding surface compared to larger silver nanoparticles or agglomerates (Rahuman et al. 2022).

This inhibition could be due to cellular induction and toxicity by generating reactive oxygen species (ROS), altering cellular translation pathways, and causing oxidative stress, that is, cellular toxicity leading to the death of the bacteria. Likewise, mechanisms of cell inhibition and death have been described due to the electrostatic interactions of Ag NPs (Rahuman et al. 2021), as can be seen in the description of the Z potential, the surfaces of the Ag NPs are negative due to the deprotonation of the functional groups of the bioactive compounds belonging to the plant extract, these molecules can adhere to the cell membrane, as well as react with the electron transport chain. According to Dakal et al. (2016), the size of the nanoparticles greatly influences the antimicrobial and bacteriostatic properties of the Ag NPs; and there may be four mechanisms of action: (1) adhesion of Ag NPs to the surface of the cell wall and membrane; (2) penetration of Ag NPs into the cell and damage to intracellular structures (mitochondria, vacuoles, ribosomes) and biomolecules (proteins, lipids and DNA); (3) cellular toxicity induced by Ag NPs and oxidative stress caused by the generation of reactive oxygen species (ROS) and free radicals; and (4) modulation of signal transduction pathways.

Conclusion

The optimization of silver nanoparticle (AgNP) synthesis enabled the identification of optimal conditions: pH 10, $AgNO_3$ concentration of 100 mM, and an extract-to-$AgNO_3$ ratio of 3:5, yielding the highest efficiency.

Under these conditions, the synthesized AgNPs exhibited an average size of 10 nm with a predominantly spherical morphology.

The synthesized nanoparticles demonstrated a negative surface charge, with larger hydrodynamic diameters (Dh) and higher agglomeration in acidic pH, whereas in basic pH, they exhibited greater dispersion, resulting in higher Dh and lower agglomeration.

At a concentration of 1000 ppm, the AgNPs exhibited 100% antimicrobial activity against *Pseudomonas aeruginosa*. However, further studies are required to evaluate their effectiveness against Gram-positive bacteria and yeasts to gain a more comprehensive understanding of their antimicrobial properties and inhibition mechanisms.

Abbreviations

Ag NPs	Silver nanoparticles
UV-Vis	Ultraviolet and visible spectroscopy
FT-IR	Fourier-transform infrared spectroscopy
DLS	Dynamic light scattering
SEM	Scanning electron microscopes
XRD	X-ray difraction
Dh	Hydrodynamic diameter
PVA	Polyvinyl alcohol
ROS	Reactive oxygen species

Authors' contributions

JBDL, methodology, formal analysis, investigation; MCLH, methodology, data curation, supervision, writing review and editing; CRRI, data curation, supervision, writing—review and editing; HOK, methodology, conceptualization; DCGD, methodology; AAG, methodology; RDO, methodology; VRE, methodology.

Funding

The authors thanks to the National Council of Arts Humanities Science and Technology (México) (1033541, JBDL scholarships) and Mexican National Technologic/Tuxtla Gutiérrez Technologic Institute (grant number 8848.20-P).

Data availability

Not applicable.

Declarations

Ethics approval and consent to participate

Not applicable.

Competing interests

The authors declare that they have no competing interests.

Author details

[1]Tecnológico Nacional de México/Instituto Tecnológico de Tuxtla Gutiérrez, KM 29020, Carr. Panamericana 1080, Tuxtla Gutiérrez, Chiapas 29050, Mexico. [2]Tecnológico Nacional de México/Instituto Tecnológico de Tijuana, Calz. del Tecnológico 12950, Tomás Aquino, Tijuana, Baja California 22414, Mexico.

Received: 20 November 2024 Accepted: 6 June 2025
Published online: 04 July 2025

References

Ahmad T, Bustam M, Irfan M, Moniruzzaman M, Asghar H, Bhattacharjee S (2017) Green synthesis of stabilized spherical shaped gold nanoparticles using novel aqueous Elaeis guineensis Jacq. (oil palm) leaves extract. J Mol Struct 1159:167–173. https://doi.org/10.1016/J.MOLSTRUC.2017.11.095

Ahmed RH, Mustafa DE (2020) Green synthesis of silver nanoparticles mediated by traditionally used medicinal plants in Sudan. Int Nano Lett 10:1–14. https://doi.org/10.1007/s40089-019-00291-9

Alharbi N, Alsubhi N, Felimban A (2022) Green synthesis of silver nanoparticles using medicinal plants: characterization and application. J Radiat Res Appl Sci 15:109–124. https://doi.org/10.1016/j.jrras.2022.06.012

Anyaoha KE, Sakrabani R, Patchigolla K, Mouazen AM (2018) Critical evaluation of oil palm fresh fruit bunch solid wastes as soil amendments: prospects and challenges. Resour Conserv Recycl 136:399–409. https://doi.org/10.1016/j.resconrec.2018.04.022

Aravind M, Ahmad A, Ahmad I, Amalanathan M, Naseem K, Mary S, Parvathiraja C, Hussain S, Algarni TS, Pervaiz M, Zuber M (2021) Critical green routing synthesis of silver NPs using jasmine flower extract for biological activities and photocatalytical degradation of methylene blue. J Environ Chem Eng 9:104877. https://doi.org/10.1016/j.jece.2020.104877

Bamal D, Singh A, Chaudhary G, Kumar M, Singh M, Rani N, Mundlia P, Sehrawat AR (2021) Silver nanoparticles biosynthesis, characterization, antimicrobial activities, applications, cytotoxicity and safety issues: an updated review. Nanomaterials 11:2086. https://doi.org/10.3390/nano11082086

Chouhan S, Guleria S (2020) Green synthesis of AgNPs using Cannabis sativa leaf extract: characterization, antibacterial, anti-yeast and α-amylase inhibitory activity. Mat Sci Ener Technol 3:536–544. https://doi.org/10.1016/j.mset.2020.05.004

Chugh D, Viswamalya V, Das B (2021) Green synthesis of silver nanoparticles with algae and the importance of capping agents in the process. J Genet Eng Biotechnol. https://doi.org/10.1186/s43141-021-00228-w

Dakal T, Kumar A, Majumdar R, Yadav V (2016) Mechanistic basis of antimicrobial actions of silver nanoparticles. Front Microbiol 7:1831. https://doi.org/10.3389/fmicb.2016.01831

Dhasarathan P, Devi N, Sangeetha P, Navaraj S, Ranjitsingh A, Padmalatha C (2018) Utilisation of green synthesised silver nanoparticles for water quality management. Adv Nanopart 07:77–84. https://doi.org/10.4236/anp.2018.74007

Dzido G, Markowski P, Małachowska-Jutsz A, Prusik K, Jarzębski A (2015) Rapid continuous microwave-assisted synthesis of silver nanoparticles to achieve very high productivity and full yield: from mechanistic study to optimal fabrication strategy. J Nanoparticle Res 17:27. https://doi.org/10.1007/s11051-014-2843-y

Dzul-Erosa MS, Cauich-Díaz M, Razo-Lazcano T, Avila-Rodriguez M, Reyes-Aguilera J, González-Muñoz M (2018) Aqueous leaf extracts of Cnidoscolus chayamansa (Mayan chaya) cultivated in Yucatán México. Part II: Uses for the phytomediated synthesis of silver nanoparticles. Mater Sci Eng C 91:838–852. https://doi.org/10.1016/j.msec.2018.06.007

Fernando I, Zhou Y (2019) Impact of pH on the stability, dissolution and aggregation kinetics of silver nanoparticles. Chemosphere 216:297–305. https://doi.org/10.1016/j.chemosphere.2018.10.122

Festus O, Emmanuella O (2020) Testing the efficacy of Mueller Hinton agar over nutrient agar for optimal antibiotic sensitivity testing response by selected clinical bacterial pathogens. GSC Adv Res Rev 5:061–074. https://doi.org/10.30574/gscarr.2020.5.2.0037

Gangwar C, Yaseen B, Kumar I, Singh N, Naik R (2021) Growth kinetic study of tannic acid mediated monodispersed silver nanoparticles synthesized by chemical reduction method and its characterization. ACS Omega 6:22344–22356. https://doi.org/10.1021/acsomega.1c03100

Gasztych M, Malamis A, Musiał W (2024) The influence of initiators, particle size and composition on the electrokinetic potential of N-(Isopropyl) acrylamide derivatives. Polymers 16:907. https://doi.org/10.3390/polym16070907

Gontijo L, Raphael E, Ferrari D, Ferrari J, Lyon J, Schiavon M (2020) pH effect on the synthesis of different size silver nanoparticles evaluated by dls and their size-dependent antimicrobial activity. Rev Mater 25:1–10. https://doi.org/10.1590/S1517-707620200004.1145

Habeeb H, Dhandapani R, Narayanan S, Palanivel V, Paramasivam R, Subbarayalu R, Thangavelu S, Muthupandian S (2022) Medicinal plants mediated the green synthesis of silver nanoparticles and their biomedical applications. IET Nanobiotechnol. https://doi.org/10.1049/nbt2.12078

Hasan W, Sari R, Hendradi E (2024) Green synthesis of antimicrobial silver nanoparticles using green tea extract: the role of concentration and pH. J Sains Farm Klin. https://doi.org/10.25077/jsfk.11.1.25-31.2024

Horiba Scientific (2022) Particle size essentials guidebook. Irvine: Horiba Scientific. https://www.horiba.com/int/scientific/products/particle-characterization/download/particle-size-essentials-guidebook-71596/

Huan E, Sin S, Koon S, Lin B, Hui S (2022) Transformation of oil palm biomass into value-added components. Rev in Agr Sci 10:36–55. https://doi.org/10.7831/ras.10.0_36

Ji J, Yao X, Ga J, Lu W, Wang W, Chu D (2021) Effect of surfactants and pH values on stability of γ-Al2O3 nanofluids. Chem Phys Lett 781:138996. https://doi.org/10.1016/J.CPLETT.2021.138996

Jiménez R, Ramírez Á, Orozco J, González M (2023) Biosíntesis de nanopartículas de plata con actividad antimicrobiana por Pseudomonas aeruginosa ambiental. Mundo Nano Rev Interdiscip Nanoci Nanotecnol 17:1e–13e. https://doi.org/10.22201/ceiich.24485691e.2024.32.69721

Kahar P, Rachmadona N, Pangestu R, Palar R, Triyono D, Betha A, Yopi MI, Hama S, Ogino C (2022) An integrated biorefinery strategy for the utilization of palm-oil wastes. Bioresour Technol 344:126266. https://doi.org/10.1016/j.biortech.2021.126266

Kiba T, Masui K, Inomata Y, Furumoto A, Kawamura M, Abe Y, Kim K (2021) Control of localized surface plasmon resonance of Ag nanoparticles by changing its size and morphology. Vacuum 192:110432. https://doi.org/10.1016/J.VACUUM.2021.110432

Klasen H (2000) A historical review of the use of silver in the treatment of burns. II. Renewed interest for silver. Burns RB Groningen 26(2):131–138. https://doi.org/10.1016/s0305-4179(99)00116-3

Lima M, De Melo G, Teixeira L, Miranda C, De Araújo P, Sayer C, Ineu R, Leimann F, Gonçalves O (2022) Green synthesis of silver nanoparticles using Ilex paraguariensis extracts: antimicrobial activity and acetilcolinesterase modulation in rat brain tissue. Green Chem Lett and Rev 15:128–138. https://doi.org/10.1080/17518253.2021.2024896

Luxbacher T (2014) The zeta potential for solid surface analysis: A practical guide to streaming potential measurement (1ª ed.). Graz, Austria: Anton Paar GmbH. https://search.worldcat.org/title/The-Zeta-potential-for-solid-surface-analysis-%3A-apractical-guide-to-streaming-potential-measurement/oclc/946020381

Mazariegos E, Valdez-Salas B, González-Mendoza D, Abdelmoteleb A, Camacho O, Ceceña Duran C, Gutiérrez-Miceli F (2019) Silver nanoparticles from Justicia spicigera and their antimicrobial potentialities in the biocontrol of foodborne bacteria and phytopathogenic fungi. Rev Argent Microbiol 51:103–109. https://doi.org/10.1016/j.ram.2018.05.002

Meher K, Garg Y, Parodi A, Lopus M (2024) Antiproliferative efficacy and mechanism of action of aggregation-resistant, polymorphous nanosilver functionalized with asparagus phytochemicals (Ar-AgNPs) in the breast adenocarcinoma MDA-MB-231 cells. Inorg Chim Acta. https://doi.org/10.1016/j.ica.2024.121960

Nabila R, Hidayat W, Haryanto A, Hasanudin U, Iryani D, Lee S, Chun D, Choi H, Im H, Lim J, Kim K, Jun D, Moon J, Yoo J (2023) Oil palm biomass in Indonesia: thermochemical upgrading and its utilization. Renew Sust Energ Rev 176:113193. https://doi.org/10.1016/j.rser.2023.113193

Nangare S, Patil P (2020) Green synthesis of silver nanoparticles: an eco-friendly approach. Nano Biomed Eng 12. https://doi.org/10.5101/nbe.v12i4.p281-296

Nelagadarnahalli H, Jacob G, Prakash D, Iska R, Iska V, Ameen F, Rajadurai U, Polachi N, Jacob J (2023) Optimization and fabrication of silver nanoparticles to assess the beneficial biological effects besides the inhibition of pathogenic microbes and their biofilms. Inorg Chem Comm. https://doi.org/10.1016/j.inoche.2023.111140

Nuchdang S, Phruetthinan N, Paleeleam P, Domrongpokkaphan V, Chuetor S, Chirathivat P, Phalakornkule C (2022) Soxhlet, microwave-assisted, and room temperature liquid extraction of oil and bioactive compounds from palm kernel cake using isopropanol as solvent. Ind Crops Prod 176:114379. https://doi.org/10.1016/j.indcrop.2021.114379

Ödemiş Ö, Özdemir S, Gonca S, Arslantaş A, Ağirtaş M (2022) The study on biological activities of silver nanoparticles produced via green synthesis method using Salvia officinalis and Thymus vulgaris. Turk J Chem 46:1417–1428. https://doi.org/10.55730/1300-0527.3448

Ofori-Boateng C, Lee K (2013) Response surface optimization of ultrasonic-assisted extraction of carotenoids from oil palm (Elaeis guineensis Jacq.) fronds. Food Sci Nut 1:209–221. https://doi.org/10.1002/fsn3.22

Ong E, Rabbani A, Habashy M, Abdeldayem O, Al-Sakkari E, Rene E (2021) Palm oil industrial wastes as a promising feedstock for biohydrogen production: a comprehensive review. Env Poll 291:118–160. https://doi.org/10.1016/j.envpol.2021.118160

Princy S, Hentry C, Alodaini H, Hatamleh A, Arokiyaraj S, Bindhu M (2023) Hibiscus cannabinus seeds assisted spherical silver nanoparticles and its antibacterial and photocatalytic applications. Chem Phys Impact 6:100192. https://doi.org/10.1016/j.chphi.2023.100192

Putri S, Oktaviana A, Rorensya C, Nurfani E, Maryanti E, Annas D, Nikmatullah M, Apriandanu D, Saputra I (2024) Effect of Elaeis guineensis Jacq. Leaf extracts concentration in the optical, structure, morphology analysis of titanium dioxide nanoparticles. Results Surf Interfaces. https://doi.org/10.1016/j.rsurfi.2024.100391

Quintero-Quiroz C, Acevedo N, Zapata-Giraldo J, Botero L, Quintero J, Zárate-Triviño D, Saldarriaga J, Pérez V (2019) Optimization of silver nanoparticle synthesis by chemical reduction and evaluation of its antimicrobial and toxic activity. Biomat Res 23:27. https://doi.org/10.1186/s40824-019-0173-y

Rahman A, Kumar S, Bafana A, Dahoumane S, Jeffryes C (2019) Biosynthetic conversion of Ag+ to highly stable Ag0 nanoparticles by wild type and cell wall deficient strains of chlamydomonas reinhardtii. Molecules 24:98. https://doi.org/10.3390/molecules24010098

Rahuman H, Dhandapani R, Palanivel V, Thangavelu S, Paramasivam R, Muthupandian S, Palanivel V (2021) Bioengineered phytomolecules-capped silver nanoparticles using Carissa carandas leaf extract to embed on to urinary catheter to combat UTI pathogens. PLoS ONE 16:e0256748. https://doi.org/10.1371/journal.pone.0256748

Rahuman HBH, Sadiq MB, Nithya C, Velayutham K (2022) Medicinal plants mediated the green synthesis of silver nanoparticles and their biomedical applications: A review. J Bionanosci 16(1):1–10. https://doi.org/10.1166/jbns.2022.1843

Rónavári A, Igaz N, Adamecz DI, Szerencsés B, Molnár C, Kónya Z, Pfeiffer I, Kiricsi M (2021) Green silver and gold nanoparticles: Biological synthesis approaches and potentials for biomedical applications. Molecules 26(4):844. https://doi.org/10.3390/molecules26040844

Rose G, Thakur B, Soni R, Soni S (2023) Biosynthesis of silver nanoparticles using nitrate reductase from Aspergillus terreus N4 and their potential use as a non-alcoholic disinfectant. J Biotech 26(4):844. https://doi.org/10.1016/j.jbiotec.2023.07.002

Saputra I, Nurfani E, Fahmi A, Saputro A, Apriandanu D, Annas D, Yulizar Y (2024) Effect of secondary metabolites from several leaf extracts on the green synthesized-ZnO nanoparticles. Vacuum. https://doi.org/10.1016/j.vacuum.2024.113434

Shantkriti S, Pradeep M, Unish KK, Viji Das MS, Nidhin S, Gugan K, Murugan A (2023) Bioynthesis of silver nanoparticles using Dunaliella salina and its antibacterial applications. Appl Surf Sci 13:100377. https://doi.org/10.1016/j.apsadv.2023.100377

Sharma S et al (2023) Chlorella minutissima-assisted silver nanoparticles synthesis and antibacterial efficacy. Biocatalysis and Agricultural Biotechnology 51:102371. https://doi.org/10.1016/j.bcab.2023.102371

Siddiqui M, Redhwi H, Achilias D, Kosmidou E, Vakalopoulou E, Ioannidou M (2018) Green synthesis of silver nanoparticles and study of their antimicrobial properties. J Polym Environ 26:423–433. https://doi.org/10.1007/s10924-017-0962-0

Smirnov O, Dzhagan V, Yeshchenko O, Kovalenko M, Kapush O, Vuichyk M, Dzhagan V, Mazur N, Kalynovskyi V, Skoryk M, Yukhymchuk V (2023) Effect of pH of Ganoderma lucidum aqueous extract on green synthesis of silver nanoparticles. Adv Nat Sci Nanosci Nanotechnol 14:035009. https://doi.org/10.1088/2043-6262/acebd4

Thakur S, Kumar P, Singh P, Shah K, Sadashivaiah B, Chauhan N (2024) Optimization, characterization of silver nanoparticles from the young leaves of Pancratium telanganense and application studies against pathogen bacteria. Curr Res Green Sustain Chem 8:100400. https://doi.org/10.1016/j.crgsc.2024.100400

Velgosova O, Mačák L, Múdra E, Vojtko M, Lisnichuk M (2023) Preparation, structure, and properties of PVA–AgNPs nanocomposites. Polymers 15:379. https://doi.org/10.3390/polym15020379

Villani S, De Matteis V, Calcagnile M, Cascione M, Pellegrino P, Vincenti L, Demitri C, Alifano P, Rinaldi R (2024) Tuning antibacterial efficacy against Pseudomonas aeruginosa by using green AgNPs in chitosan thin films

as a plastic alternative. Int J Biol Macromol 285:1382. https://doi.org/10.1016/j.ijbiomac.2024.138277

Wang X, Lee S-Y, Akter S, Huq MA (2022) Probiotic-mediated biosynthesis of silver nanoparticles and their antibacterial applications against pathogenic strains of Escherichia coli O157:H7. Polymers 14(9):1834. https://doi.org/10.3390/polym14091834

Xiong Y, Liu X, Xiong H (2021) Aggregation modeling of the influence of pH on the aggregation of variably charged nanoparticles. Sci Rep 11:17386. https://doi.org/10.1038/s41598-021-96798-3

Publisher's Note

Springer Nature remains neutral with regard to jurisdictional claims in published maps and institutional affiliations.